

RSC Advances



This is an *Accepted Manuscript*, which has been through the Royal Society of Chemistry peer review process and has been accepted for publication.

Accepted Manuscripts are published online shortly after acceptance, before technical editing, formatting and proof reading. Using this free service, authors can make their results available to the community, in citable form, before we publish the edited article. This *Accepted Manuscript* will be replaced by the edited, formatted and paginated article as soon as this is available.

You can find more information about *Accepted Manuscripts* in the [Information for Authors](#).

Please note that technical editing may introduce minor changes to the text and/or graphics, which may alter content. The journal's standard [Terms & Conditions](#) and the [Ethical guidelines](#) still apply. In no event shall the Royal Society of Chemistry be held responsible for any errors or omissions in this *Accepted Manuscript* or any consequences arising from the use of any information it contains.

ARTICLE

A versatile binder-free TiO₂ paste for dye-sensitized solar cells

Cite this: DOI: 10.1039/x0xx00000x

Jeremy H. Yune,^a Inna Karatchevtseva,^a Peter J. Evans,^a Klaudia Wagner,^b Matthew J. Griffith,^b David Officer^b and Gerry Triani^{*a}

Received 00th January 2012,
Accepted 00th January 2012

DOI: 10.1039/x0xx00000x

www.rsc.org/

In this study, binder-free TiO₂ colloidal pastes have been prepared using a variety of heterocyclic bases with diverse characteristics to produce robust photoanodes for dye-sensitized solar cells (DSSC) from a single cast film thickness of 5 micron. The influence of the base on the electrode structure and film morphology, including its electron donor characteristics are investigated after low temperature thermal treatment and high temperature sintering. Results show quinoline in the TiO₂ paste is retained within the electrode structure in comparison to piperidine and pyridine after a short thermal treatment of 150°C for 15 minutes. The presence of organic additives with π -conjugation in the photoanode enhances both electron injection efficiency and charge carrier lifetime resulting in higher *J*_{sc} and *V*_{oc}. This formulation in combination with low temperature processing yields an energy conversion efficiency of over 5% in DSSC devices. In devices where high temperature sintering is permitted, the performance of TiO₂ electrodes converges towards an efficiency of over 6%, irrespective of the organic additive within the paste. This formulation offers a high degree of versatility in casting electrodes onto polymer, glass or metal foil substrates from a single source of TiO₂ paste, for the many variants of low-cost solar cells.

Introduction

One of the major global challenges over the next 40 years will be to fulfil the rising energy demands from emerging countries and an increasing population.¹ Solar generation has the potential to contribute a large proportion of the renewable energy required for the projected 30 terawatts by 2050.^{2,3} However, in order for solar to achieve better penetration into the energy sector, a more competitive cost structure is required to lower the cost of manufacture.⁴ Dye-sensitized solar cells are a promising low-cost third generation photovoltaic device where both components and manufacturing processes are relatively cheaper in comparison to silicon based devices⁵ and have demonstrated energy conversion efficiency of over 10%⁶ coupled with good performance over a broad range of light intensity levels.^{7,8}

Since the pioneering work of O'Regan and Gratzel in 1991,⁹ dye-sensitized solar cells (DSSC) have created enormous interest in the research community, where improvements in both materials and process technologies have been addressed along with enhancements in device architecture.

These developments have translated into an exponential rise in peer-review articles¹⁰ resulting in performance improvements, which have yielded devices with energy conversion efficiencies of 15%.¹¹ One of the prime areas of research has been the development of TiO₂ electrodes in DSSC, which are typically deposited as a continuous film from a

viscous paste. TiO₂ paste is prepared with organic binders, which modify the rheology for coating and impart porosity in the thick film structure.

Conducting glass substrates are used as the support and these allow thermal process treatments at temperatures >400°C to ensure organics are eliminated and to improve particle binding and adhesion to the substrate.⁶ A key driver in cost reduction of the DSSC is the replacement of glass-based substrates with polymers that are amenable to continuous roll-to-roll processing.^{12,13} Low temperature mesoporous TiO₂ films for photoanodes on polymers require processes less than 150°C with acceptable particle connectivity for electron diffusion. Several methods have been reported as low temperature processes with additional steps following TiO₂ film formation. They include immersion with TiCl₄,¹⁴ UV-O₃ curing,¹⁵⁻¹⁷ TiO₂ atomic layer deposition¹⁸ or compression.¹⁹ All of these studies show improvements in performance after TiO₂ film deposition, with the best recorded efficiency of 7.6%²⁰ on ITO/PEN achieved by compression coupled with UV-O₃ curing post film formation. However, integration of such a process in DSSC device fabrication remains challenging¹² where a singular process step following deposition with minimal resident time is preferred.¹³

Casting of TiO₂ from a viscous vehicle onto substrates is by far the preferred method of depositing electrodes for DSSC.^{12,21} However, additives for low temperature TiO₂ paste must provide adequate viscosity and volatility in order to yield

uniform porous structures. An interesting method reported by Park et al.^{22,23} utilises a binder-free formulation by adding small quantities of ammonia solution into an acidic TiO₂ aqueous sol. Surface mediated CH₃COO⁻/NH₄⁺ couples are formed within the slurry, which results in the reduction of the double layer repulsion between the particles; as a result this induces TiO₂ particles to flocculate sufficiently to allow uniform films to be cast.

In our previous study,²⁴ the influence of acetate molar ratio within the acidic TiO₂ colloid was investigated in low temperature processing of electrodes in DSSC. Lowering the molar ratio of TiO₂ to CH₃COOH in the starting colloid and the amount of ammonia in the paste formation, followed by low temperature processing at 150°C for 15 minutes, resulted in the energy conversion efficiency of the DSSC increasing from 2.83 to 5.00% in comparison to Park's results.^{22,23} Further incremental improvements were possible after the electrodes were heat treated at 150°C for 24 hours.

Huang²⁵ and Boschloo²⁶ have both reported enhancements in device performance by the addition of particular nitrogen-containing compounds to the electrolyte solution. For example, the use of 4-*tert*-butylpyridine (TBP) as documented in the literature enhances the performance of the cell by improving the open-circuit voltage but at the expense of *J*_{sc}.²⁵ The proposed mechanism is that TBP binds to either a TiO₂ surface or electrolyte via the nitrogen atom thus protecting it against the charge recombination. The basic nature and electron donor properties of various heterocyclic amines within the electrolyte have been identified to be responsible of TiO₂ conduction band shift and therefore influence DSSC characteristics.²⁷⁻³¹

In this study, we investigate the incorporation of a variety of bases with diverse characteristics, including basicity, boiling point and electrochemical properties. TiO₂ colloidal pastes were formulated using heterocyclic amines during paste preparation as opposed to addition within the electrolyte, with anticipation that this functional moiety will have a higher probability of binding to a TiO₂ surface, hence reducing back electron transfer. This study seeks to establish a relationship between electron donor characteristics of the base in the TiO₂ electrode and the solar cell performance of DSSCs prepared with several amines; piperidine, pyridine and quinoline. In order to best compare the high temperature and low temperature paste performance in DSSCs, we have fabricated DSSCs with a single nanocrystalline TiO₂ layer on a glass photoanode without the usual blocking layer (Figure 1).

Experimental

Preparation of TiO₂ paste

TiO₂ solutions were prepared using a method reported by Karatchevtseva et al.³² Briefly, 85 mL of titanium (IV) isopropoxide was mixed with 17.4 g of glacial acetic acid (1:1 mol ratio) in a glove box under inert conditions and vigorous stirring. This solution was slowly added via a dropping funnel to 512 g of H₂O under vigorous stirring for 10 minutes at room temperature followed by the addition of 5 mL of nitric acid (concentration 69%), used as a peptization agent.^{33,34} The reaction mixture was heated at 80°C under vigorous stirring for 8 hours. TiO₂ sol was converted into highly crystalline anatase via a hydrothermal procedure by introducing 150 g of TiO₂ sol into a 200 mL titanium autoclave heated to 240°C, which was controlled by ramping at 2°C/min and held at temperature for

14 hours. An aqueous TiO₂ suspension of anatase with uniform particle size distribution was collected after ultra-sonication for 15 minutes followed by centrifugal separation at a rotation speed of 3000 min⁻¹ for 15 minutes.

Binder-free TiO₂ paste was prepared by adding a calculated quantity of dilute 2M basic solution to an acidic anatase TiO₂ colloid where the final weight percentage of TiO₂ was 21%. This was determined after thermogravimetric analysis where the amount of base (piperidine, pyridine and quinoline) was in the range 1.7-2.1 wt.% with respect to TiO₂. Viscous pastes were ready for casting after 2 hours of agitation.

DSSC preparation

The TiO₂ photoanode films were deposited by casting onto either microscope soda lime glass slides or indium doped tin oxide (ITO) coated on glass substrates (Asahi, Sheet Resistance: $R_s \leq 8 \Omega \text{ sq}^{-1}$) using the doctor blade technique. The thickness of a single cast dried TiO₂ electrode was $5.0 \pm 0.2 \mu\text{m}$. The TiO₂ films were first air dried for 30 minutes and then heat-treated on a hot plate at either 150°C for 15 minutes for low temperature devices or processed at 450°C for 30 minutes. The active electrode area was 0.25 cm^2 . Prior to assembly into DSSC devices, the TiO₂ films were further treated for 2 hours at 120°C on a hot plate, in order to remove most of physisorbed water, and immersed while hot into 0.3 mM anhydrous *cis*-diisothiocyanato-bis(2,2'-bipyridyl-4,4'-dicarboxylato) ruthenium (II) bis-(tetrabutylammonium) (N719 dye purchased from Solaronix SA Ltd.) solution in acetonitrile/*tert*-butyl alcohol (1/1) for 22 hours. The sensitized TiO₂ electrode was sandwiched with a Pt-sputtered (~30 nm thickness) indium tin oxide (ITO)-glass counter electrode (Delta Technologies, $R_s \sim 10 \Omega \text{ sq}^{-1}$) spaced with a 25 μm Surlyn sealant (Figure 1). An electrolyte solution comprising 0.6 M 1,2-dimethyl-3-propylimidazolium iodide (DMPH), 0.5 M 4-*tert*-butylpyridine, 0.1 M LiI, and 0.05 M I₂ in a solvent mixture of 85:15 acetonitrile/valeronitrile was injected between the electrodes through a hole in the counter electrode by a vacuum-filling procedure. Four samples were prepared for every condition investigated.

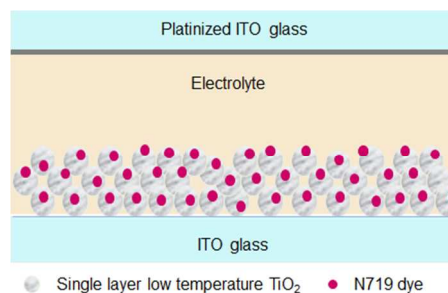


Fig. 1 Schematic diagram of the DSSC structure used in these studies.

TiO₂ Film Characterisation

The thickness of both dried and thermally treated TiO₂ films on glass were measured using the Alpha-Step IQ Surface Profiler (KLA-Tencor). Further, measurements of film transmittance

were recorded by UV-Vis spectroscopy on a Perkin Elmer Lambda 35 UV-Vis spectrometer.

Specific surface areas of the as-prepared and post-treated TiO₂ electrodes were measured by the Brunauer-Emmett-Teller (BET) nitrogen adsorption method. Cast films were removed from their substrates by scratching and placing contents into glass bulbs for measurement. Nitrogen adsorption isotherms at 77 K were measured on a Quantachrome AutoSorb iQ volumetric adsorption analyzer.

Scanning electron microscopy (SEM) provided a comparative study of TiO₂ film morphology. Samples were examined by field emission SEM (Zeiss Supra 55VP) operating at an accelerating voltage of 10 kV. Films were mounted on a conductive carbon adhesive and approximately 30 Å of platinum was evaporated onto the surface to prevent charging.

Fourier transform infrared (FTIR) spectra were obtained on a Nicolet Nexus 8700 FTIR spectrometer (Thermo Electron Corporation, Madison, WI). Both dried and thermally treated films were measured using the Smart iTR™ sampling accessory to observe the presence of residual organics. Spectra were collected by averaging 32 scans with a nominal resolution of 4 cm⁻¹.

DSSC Characterisation

Current-voltage curves were recorded using a Keithley 2400 source measure unit after illuminating the DSSCs with a simulated 100 mW cm⁻² air mass AM 1.5 light source (Oriol) equipped with a KG5 filter to remove longer wavelengths. The light intensity was adjusted using a calibrated silicon diode (Peccell). The device area was masked with black paint defining an aperture slightly larger than the active area.³⁵ The light intensity of the simulated sunlight source was reduced for specific measurements using neutral density filters. Incident photon-to-current conversion efficiency (IPCE) spectra were recorded on a home-built set-up using the monochromated output from a xenon lamp equipped with sorting filters. The output beam was focused to a spot size smaller than the DSSC area. The short circuit current response of devices was recorded in 5 nm steps using the aforementioned Keithley 2400 instrument referenced to the output of a calibrated silicon diode (Peccell).

Electron lifetime and diffusion coefficient measurements were performed using stepped light-induced recording of photocurrent and photo-voltage (SLIM-PCV) transients.³⁶ Measurements were performed using a 635 nm diode laser illuminating the entire DSSC active area. This wavelength was selected as the dyes are weakly absorbing at 635 nm, allowing a uniform generation of electron density throughout the entire TiO₂ film thickness. The illumination intensity of the laser, controlled by the input voltage, produced values ranging from 2 mW cm⁻² to 35 mW cm⁻². Photocurrent and photovoltage transients were induced by the small stepwise (≤10%) change of the laser intensity, controlled with a PC using a digital-to-analogue converter. Induced transients were measured by a fast multimeter (AD7461A, Advantest). Electron densities at specific laser illumination intensities were determined by a charge extraction method in which the light source was switched off at the same time the DSSC device was switched from open to short circuit.³⁵ The resulting current was integrated, with the electron density calculated from the amount of charge extracted. Diffusion coefficients were determined by fitting the current decays to a single exponential as previously

reported,³⁶ although we note that this treatment neglects potential recombination losses during charge transport. Electron lifetimes were determined by fitting the voltage transients to single exponential decays as previously reported.³⁶

The electrochemical data were obtained using square wave voltammetry in anhydrous acetonitrile containing 0.1 M tetrabutylammonium perchlorate (TBAP) as supporting electrolyte. The working electrodes were indium tin oxide (ITO) slides with N719-sensitised TiO₂. Solutions were degassed prior to measurement and ferrocene was added as an internal reference. Pt mesh and Ag/Ag⁺ electrode were used as the counter electrode and quasi-reference electrode respectively. Half-wave potential was measured for 1 mM ferrocene, E_{1/2} = 0.21 V, vs. Ag/Ag⁺ reference electrode. The results were recorded using an eDAQ potentiostat system controlled by eDAQ EChem software. Solutions were degassed prior the measurements.

HOMO potentials were estimated from the oxidation half-wave potential (E_{1/2}^{ox}) of the anodic peak. The optical band gap was estimated from UV-Vis absorption spectra of the samples prior to electrochemistry. The LUMO potentials for both dyes were then estimated by subtracting the optical band gap value from the HOMO potential.

Fluorescence spectra were recorded with a Horiba Scientific Fluorolog Model FL 3-221 spectrofluorometer system.

Results and discussion

TiO₂ pastes were formulated with the addition of a heterocyclic base to the starting acidic TiO₂ colloid and processed according to our previous study.²⁴ Briefly, the base reacts with residual acetic acid groups and forms a salt. An increase in ion concentration between the acid⁻/base⁺ couple promotes a decrease of the double layer repulsion between TiO₂ nanoparticles thereby contributing to flocculation, which results in the formation of a viscous slurry. A similar behaviour was reported in our previous study where an optimum weight ratio between the additive base and TiO₂ content was defined. A similar approach was undertaken in this study.

TiO₂ films properties

The presence of organics was monitored by Fourier-Transform Infrared (FTIR) spectroscopy. FTIR spectra of piperidine, pyridine and quinoline-based TiO₂ as-prepared films are shown in Figure 2. Several common IR adsorption bands were observed in each sample. Firstly, the broad band below 800 cm⁻¹ is due to the formation of an extensive inorganic Ti–O–Ti network. A broad peak centred at ~1630 cm⁻¹ indicates the presence of Brønsted acidity (the O–H groups residing on TiO₂ surface) in all samples. While another broad doublet peak centred between 1500 and 1300 cm⁻¹ is indicative of the Lewis acidity.

The nature of acid sites may be defined by the presence of surface protons leading to the Brønsted sites or cationic centres due to unsaturation in coordination, which explains the Lewis acidity. These sites can potentially serve as the adsorption sites for organic species. For example, Miyata *et al.*³⁷ observed a broad band in the region 1300 – 1400 cm⁻¹ in their study of pyridine adsorbed on transition metal oxides. Dines *et al.*³⁸

have reported bands at similar wavenumbers in the case of quinoline chemisorbed onto TiO₂ surface.

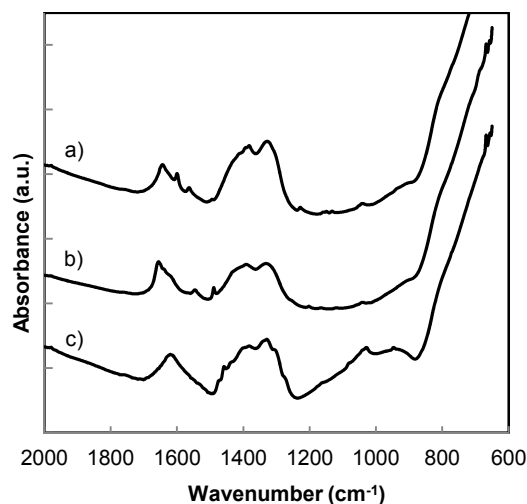


Fig. 2 FTIR spectra of as-prepared TiO₂ films synthesised using: a) quinoline, b) pyridine and c) piperidine.

There are also several IR bands found in each spectrum that are unique to each sample. For example, quinoline typically has 3 characteristic bands (due to aromatic ring vibration) near 1600 cm⁻¹, two of which, 1600 and 1565 cm⁻¹, can clearly be seen in the spectrum (Figure 2 a). In pyridine (Figure 2 b), the interactions between ring C=C and C=N stretching vibrations result in two absorption bands found at 1546 and 1489 cm⁻¹, respectively.³⁹ Piperidine has a distinct absorption band at 1028 cm⁻¹ that has been assigned to the C–N stretching vibration (Figure 2 c).

After casting the TiO₂ paste into thick films, electrodes were heat treated at 150°C to prepare the anode for subsequent solar cell fabrication. FTIR spectra of TiO₂ films treated at 150°C for 15 minutes are shown in Figure 3. The IR data indicated that only the quinoline-based film retained most of its organic component after this heat treatment, with characteristic bands distinguishable in the spectrum (Figure 3 a).

In contrast, the intensity of IR bands for both pyridine and piperidine treated at 150°C for 15 minutes (Figure 3 b and c) have significantly decreased compared to the corresponding as-prepared films. This is due to desorption of pyridine or piperidine since their boiling points are around 115 and 106°C, respectively. In comparison, the spectrum of the quinoline based paste shows little change following treatment at 150°C as the boiling point of quinoline is 238°C.

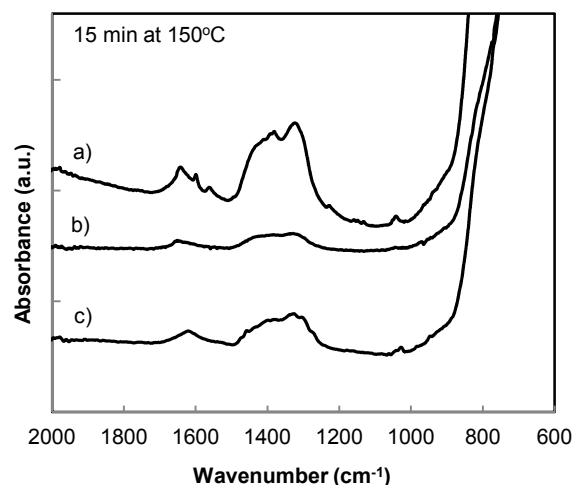


Fig. 3 FTIR spectra of TiO₂ films synthesised using: a) quinoline, b) pyridine and c) piperidine after heat treated at 150°C for 15 min.

After continuous heat treatment at 450°C for 30 min all three samples produced almost identical IR spectra (Figure 4N). Firstly, a minor peak is evident in all samples in the range 1020–1015 cm⁻¹ and attributed to a residual carbon. The CHN microanalytical analysis indicated the atomic percentage of carbon for quinoline, pyridine and piperidine-based films heat treated at 450°C for 30 min were 0.15, 0.19 and 0.18, respectively. Secondly, the presence of a weak broad peak at 1640 cm⁻¹, corresponding to O–H deformation, indicates that surface bonded hydroxyl groups were still present even after the heat treatment at 450°C. This suggests the chemical functionality of the TiO₂ surface appears largely unchanged after the prescribed thermal treatments.

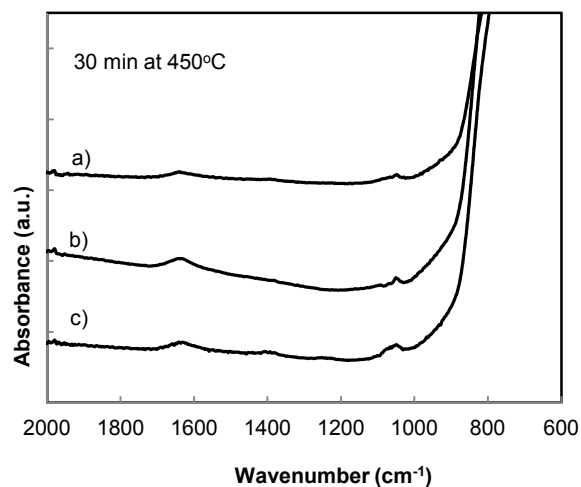


Fig. 4 FTIR spectra of TiO₂ films synthesised using: a) quinoline, b) pyridine and c) piperidine after heat treated at 450°C for 30 min.

It is well established that the TiO₂ photoanode microstructure affects the maximum amount of dye loading on the TiO₂ electrodes, in addition to influencing device physics such as electron diffusion and charge carrier lifetime. Moreover, several reports suggested that the mesoscopic structure of the TiO₂ electrodes had a major influence on the

performance of DSSCs.⁴⁰⁻⁴² Surface area and porosity as well as particle size distribution and film preparation procedure^{43,44} could all have a major influence on film morphology and therefore affect the structure of TiO₂ electrode. Thus in this work the morphologies of TiO₂ films prepared using different bases and post-treatment conditions were carefully studied.

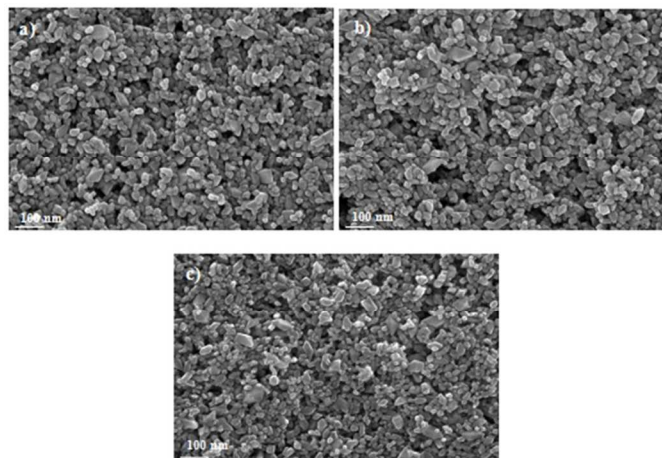


Fig. 5 SEM images of a) piperidine, b) pyridine and c) quinoline-based TiO₂ films after 15 minutes at 150°C

Figure 5 shows plan view SEM images of titania films prepared using different pastes. The morphology of the resulting TiO₂ films produced after heat treatment at 150°C for 15 minutes appears to be similar, showing uniform porosity and interconnected nanoparticles throughout the film.

Nitrogen sorption analysis was used to assess the effect of different heterocyclic bases have on TiO₂ film formation and porosity of the cast electrodes. A summary of this analysis detailing surface area and porosity of cast electrodes is presented in Table 1. Nitrogen adsorption-desorption isotherms for TiO₂ films post treated at 150°C for 15 minutes and 450°C at 30 minutes (not shown) have designated Type IV isotherms using the IUPAC classification scheme.⁴⁵

Table 1 Summary of nitrogen sorption analysis for TiO₂ films

Films	Heat treatment	Surface area (m ² /g)	V pores ¹⁾ (cm ³ /g)	D pores ²⁾ (nm)	Porosity ³⁾ (%)
Piperidine	15	85.3	0.253	11.9	49.6
Pyridine	minutes	87.5	0.252	11.5	49.5
Quinoline	at 150°C	80.4	0.254	12.6	49.7
Piperidine	30	79.7	0.245	12.3	48.8
Pyridine	minutes	77.6	0.246	12.7	48.9
Quinoline	at 450°C	75.8	0.237	12.5	48.0

¹⁾ Single-point total pore volume of pores at P/P₀ > 0.99,

²⁾ Average pore diameter (4V/A by BET),

³⁾ P = V/(ρ⁻¹ + V), ρ – density of anatase (ρ⁻¹ = 0.257 cm³/g)

The isotherms in each heat-treatment group were of similar shape and all exhibited a narrow type H1 hysteresis loop over the relative pressure range 0.80-1.0, associated with the capillary condensation in mesopores. Surface area values estimated by the BET method for all films treated at 150°C for 15 min were in the range 80.4 – 87.5 m²/g and total pore volume 0.252 – 0.254 cm³/g. A decrease in both surface area and pore volume was observed after sintering at 450°C which was attributed to nanoparticle necking. These characteristics are comparable to low and high temperature TiO₂ electrodes developed by Miyasaka et al.⁴⁶ and Ito et al.,⁶ respectively.

Overall, very little difference in film morphology could be observed between the bases studied, suggesting that the nature of the bases used during the paste formulation does not influence significantly the microstructure of the TiO₂ electrodes.

DSSC performance

TiO₂ electrodes were cast using additives piperidine, pyridine or quinoline formulated in pastes, followed by heat treatment to 150°C. TiO₂ blocking layers were not used in the preparation of these devices. Since the porosities of the high and low temperature pastes are similar (Table 1), the back transfer recombination reaction between electrons in the ITO electrode and electrolyte ions penetrating through the TiO₂ pores should also be similar for both types of paste, allowing for an accurate comparison of the pastes. Cells were prepared after sensitization with ruthenium dye N719. Table 2 records DSSC performance after both low (150°C) and high temperature (450°C) treatment of films prepared with different heterocyclic bases: piperidine, a six membered ring amine; pyridine, a six membered ring amine with π-conjugated electron and quinoline films, which is more electron rich compared to pyridine via the supplementary aromatic. The order of basicity is as follows: piperidine > pyridine > quinoline.⁴⁷ Previously FTIR spectra suggested different amounts of base were retained within TiO₂ electrodes after heat treatment at 150°C for 15 minutes since the boiling point of piperidine and pyridine is lower than this temperature. In order to study the influence of the base, which is responsible for the characteristic response in DSSC performance, films were prepared and performance tested without heat treatment where an equivalent amount of additive with a weight ratio of base to TiO₂ was between 1.7 and 2.1 wt. %.

Table 2 summarises the DSSC performance data as a function of heat treatment. All films under investigation were approximately 5 μm thick. The V_{oc} values for the as-prepared piperidine, pyridine and quinoline films were recorded at 753, 760 and 772 mV, respectively. This trend is in good agreement with previous results from Kusama et al.²⁷ where similar bases were adsorbed onto the TiO₂ surface from the electrolyte solution. In this study the changes were ascribed to modification of the TiO₂ conduction band, in accordance with other literature. Such shifts of the conduction band typically result in reduced device photocurrent as the driving force for charge injection between the dye LUMO and the TiO₂ conduction band is reduced.²⁵ However, in our study we observed that J_{sc} increases corresponding to increases in the π-electron strength of the bases. The J_{sc} improved significantly from 4.84, 7.51 to 8.12 mA/cm² for piperidine, pyridine and quinoline additions to films, respectively. This result

demonstrates a simultaneous increase of both V_{oc} and J_{sc} after addition of a more basic and π electron rich amine to a DSSC. As a result, the overall DSSC performance increased from 2.62% for piperidine to 4.25% for pyridine and 4.63% for quinoline as-prepared films.

Table 2 Influence of heat treatment on DSSC performance for 5 μm TiO_2 electrodes prepared with piperidine, pyridine and quinoline. Γ – dye surface concentration, [$\text{mol cm}^{-2} \mu\text{m}^{-1}$]. Average data for 4 devices.

Set	Heat treatment	V_{oc} [mV]	J_{sc} [mA/cm^2]	FF	η [%]	Γ
 Piperidine films	No heat treatment	753	4.84	0.72	2.62	
	15 minutes at 150°C	743	7.95	0.72	4.21	1.8×10^{-8}
	30 minutes at 450°C	745	12.3	0.69	6.37	1.6×10^{-8}
 Pyridine films	No heat treatment	760	7.51	0.75	4.25	
	15 minutes at 150°C	755	8.63	0.73	4.76	1.9×10^{-8}
	30 minutes at 450°C	745	12.1	0.70	6.30	1.6×10^{-8}
 Quinoline film	No heat treatment	772	8.12	0.74	4.63	
	15 minutes at 150°C	760	9.39	0.75	5.35	1.6×10^{-8}
	30 minutes at 450°C	750	12.5	0.68	6.38	1.5×10^{-8}
Solaronix reference	30 minutes at 450°C	736	11.9	0.65	5.76	

Conventional thermal treatment at 150°C for 15 minutes particularly affects the performance characteristics of TiO_2 electrodes with heterocyclic additives (Table 2). The V_{oc} decreased following elimination of the corresponding base which shifts the TiO_2 conduction band, resulting in a drop of 1.32, 0.66 and 1.55% for piperidine, pyridine and quinoline respectively. However, under this thermal regime TiO_2 particle interconnectivity occurs through dehydration of surface hydroxyls to form $\text{Ti}-\text{O}-\text{Ti}$ bridges.^{22,24} The formation of these bridges results in a significant rise in J_{sc} in all electrodes by 64, 15 and 16% for piperidine, pyridine and quinoline, respectively. Consequently an increase in energy conversion efficiencies of 4.21, 4.76 and 5.35% were recorded for devices with additives piperidine, pyridine and quinoline, respectively. In an attempt to improve energy conversion efficiency, the amount of quinoline additive was altered as a function of TiO_2 however performance remained equivalent after doubling the quantity within the paste.

On heat treatment to 450°C, the TiO_2 particles undergo sintering to form robust electrodes. Both the J_{sc} and energy conversion efficiencies of all cells from the additives studied converged to $12.3 \pm 0.2 \text{ mA}/\text{cm}^2$ and $6.3 \pm 0.1\%$, respectively (Table 2). This result is attributed to necking of the TiO_2 nanoparticles, a reduction of defects in the semiconductor bulk, and the removal of organics at higher temperatures.

Table 2 shows a simultaneous increase of both V_{oc} and J_{sc} with more basic or richer π -conjugated electron heterocyclic amine after no treatment and 15 minutes at 150°C, suggesting that different surface interactions occur between the base and semiconductor and that electron transfer kinetics between the various DSSC components (TiO_2 , dye, electrolyte) occur when base is added during paste formulation in comparison to additions in the electrolyte.

Furthermore, dye surface concentrations were computed as $\Gamma = A/0.001\epsilon$ from the absorbance data and scaled for the film thickness.⁴⁸ Minimal variation in surface coverages was observed between the three different pastes (Table 2), consistent with their similar surface areas as determined by BET measurements (Table 1). The dye forms layers with 75–95% of full monolayer coverage based on a value of $2 \times 10^{-8} \text{ mol cm}^{-2} \mu\text{m}^{-1}$ for full coverage.⁴⁹

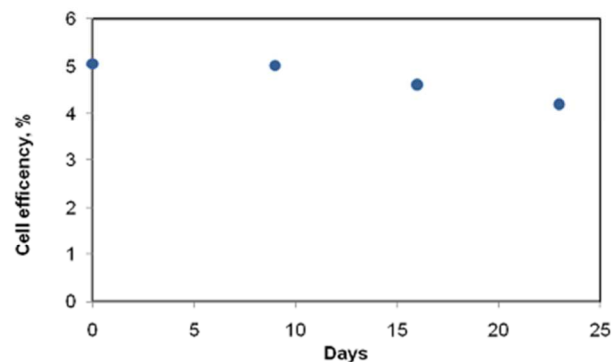


Fig. 6 Cell efficiency averaged over 4 cells produced from the quinoline based paste monitored over 25 days.

The efficiency of four cells prepared using the quinoline based paste were tested at intervals over a 25 day period and the averaged results are shown in Figure 6. An average decrease in efficiency of ~17% has occurred during the test period. Similar changes were recorded for cells produced from pastes prepared with pyridine and piperidine. This temporal decline in cell performance will be examined in more detail in future work.

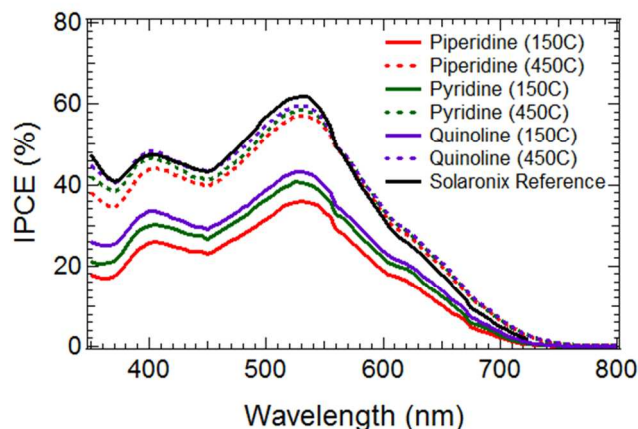


Fig. 7 IPCE of different TiO_2 electrodes heat treated at 150°C and 450°C.

The device J_{sc} is determined from a combination of the efficiencies for light harvesting, electron injection and electron collection at the anode. In order to determine if the base in the film can improve light harvesting and potentially transfer its energy to TiO_2 electrodes via direct charge transfer (DCT), film transmittance and the absorption spectra of the bases in solution were measured and correlated with the device incident photon-to-current conversion efficiency (IPCE) spectra. Although the π -aromatic bases do absorb light within the range 280–350 nm,

UV-Vis spectra recorded from the different TiO₂ films, at equivalent thickness, show different transmittance intensities; however there were no new absorption bands. Moreover, IPCE spectra, exhibited in Figure 7, obtained with TiO₂ electrodes sensitized with N719 show identical spectral shapes with no new bands characteristic samples preparation. We note that these IPCE spectra were measured on devices made with thin (2 μm) TiO₂ films prepared for further spectroscopic studies (vide infra), and thus do not match the *J*_{sc} data presented in Table 2. Integration of the overlap between the area under the IPCE spectra in Figure 7 and the AM 1.5G solar spectrum does however exhibit good agreement with the *J*_{sc} values measured for these thin film devices (Figure 8b). Furthermore, the ratio of *J*_{sc} values between the three TiO₂ pastes in the thin film devices show excellent correlation with the ratio of *J*_{sc} values observed for the three TiO₂ pastes in the devices with thicker 5 μm films (Table 2), which indicates the device performance trends for the thin film devices are representative of the trends in the 5 μm film devices discussed earlier. This result suggests that direct charge transfer from base additive is not apparent or at most, is not significant; therefore this observed phenomenon cannot alone explain the increases in *J*_{sc}.

To further investigate the *J*_{sc} changes in each electrode, the efficiency of charge injection from photo excited dyes into the TiO₂ electrode (ϕ_{inj}) was determined by a measuring the absorbed photon to current conversion efficiency (APCE) of thin TiO₂ electrodes (up to 2 μm). At this thickness, electron collection efficiency (ϕ_{cc}) is considered to be quantitative, and thus the APCE is indicative of the injection efficiency as described in the equations below:

$$IPCE = LHE \phi_{inj} \phi_{cc}$$

where LHE is the efficiency of light absorption by the dye.

Thus:

$$APCE = IPCE/LHE = \phi_{inj} \phi_{cc}$$

The APCE in the wavelength range of 380-620 nm, characteristic of the N719 dye absorption, of thin TiO₂ electrodes are shown in Figure 8 a.

Throughout this range, at low temperature, the APCE of samples prepared using quinoline was higher than pyridine, both of which exhibit higher values than piperidine TiO₂ films. After sintering electrodes at 450°C, where no organics remain within the films, the APCE of the different electrodes increased and exhibit identical values close to 100 %. The APCE of these electrodes was also comparable to the one prepared from a reference device made from Solaronix paste and sintered at 450°C. This is in agreement with previous measurements which suggest that the electron injection efficiency of N719 dye on this TiO₂ is close to unity.^{50,51} This result suggests that the APCE technique employed here is an accurate way to probe the injection yield of devices. A linear relationship was found between the APCE (averaged across the spectral range) and the device *J*_{sc}, as shown in Figure 8 b. This provides further support to the assertion that the increased *J*_{sc} with the π -electron rich bases is likely due to the increase of APCE, and consequently electron injection.

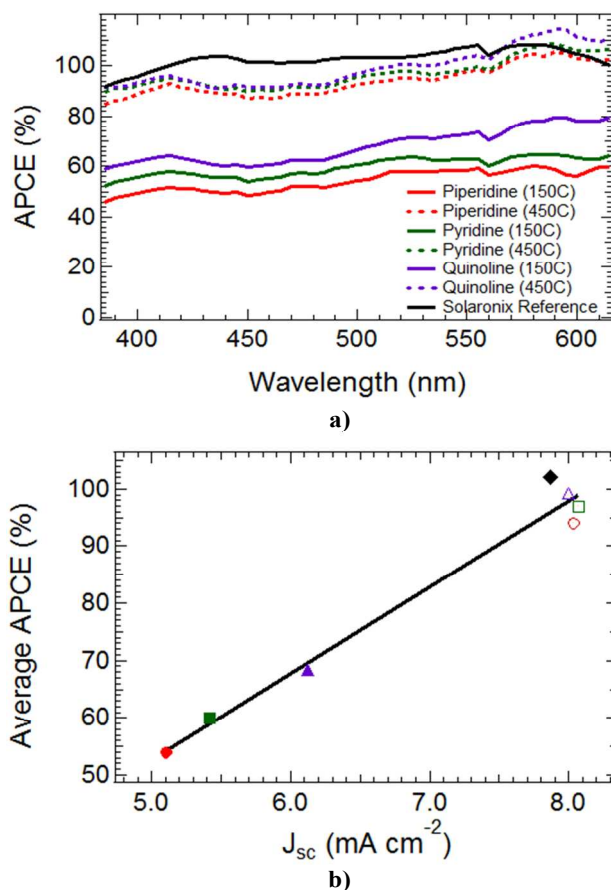


Fig. 8 a) APCE of different TiO₂ electrodes heat treated at 150°C and 450°C; b) Plot of average APCE vs. *J*_{sc} of TiO₂ electrode.

The most commonly observed cause of changes in the injection efficiency of DSSCs is a shift in the relative driving force between the dye LUMO and the TiO₂ conduction band which influences the electronic overlap between the semiconductor acceptor states and the dye LUMO. To analyse whether this driving force changes with different organic bases, we first measured the dye LUMO level on TiO₂ films prepared with each base using cyclic voltammetry to estimate the dye HOMO and the absorbance onset of N719 to determine the HOMO-LUMO gap. The bases in the TiO₂ electrode were observed to have little influence on the HOMO and LUMO energies of the dye. Thus the driving force for injection is not affected by changes in the dye LUMO. To determine whether the TiO₂ conduction band is shifted in the presence of different bases, the relative conduction band edges were determined from transient photovoltage and charge extraction measurements (Figure 9).

The open circuit voltage (*V*_{oc}) of DSSCs was determined by the difference between the quasi-Fermi level of electrons in the nanocrystalline TiO₂ in the dark and under illumination. Given the high density of states in the redox mediator, its potential shifts by only ~1 mV under illumination, thus the *V*_{oc} can be practically defined as the difference between the TiO₂ Fermi level and the Nernst potential of the redox electrolyte under illumination. Since the redox mediator is constant in all samples, the *V*_{oc} versus electron density plots in Figure 9 are indicative of the relative conduction band edge potentials in

each device if the energy difference between the Fermi level and conduction band edge remains constant. At 150°C, the TiO₂ conduction band therefore shifts positively (with respect to an NHE reference potential) in the order piperidine < pyridine < quinoline (most positive). This positive shift corresponds to the trend in basicity of the heterocyclic amines used. This shift would cause an increase in the driving force between dye LUMO and TiO₂ conduction band for the more π -electron rich bases, and can therefore help explain the improvement in device J_{sc} observed for samples prepared from the more π -electron rich bases. Furthermore, the V_{oc} vs electron density plots are coincident at 450°C once the base is removed, supporting the identical J_{sc} observed in these samples. We note that the slope of the plots in Figure 9 appears to change when comparing the samples heated to 150°C and heated to 450°C. Since this slope is indicative of the density of trap states in the TiO₂, this result suggests that the density of trap states changes after removal of the bases from the TiO₂. It is therefore likely that bases contribute to trap states in the TiO₂. Consequently, whilst the J_{sc} is improved by a conduction band shift increasing the driving force for charge injection, it could also be influenced by these traps in the TiO₂.

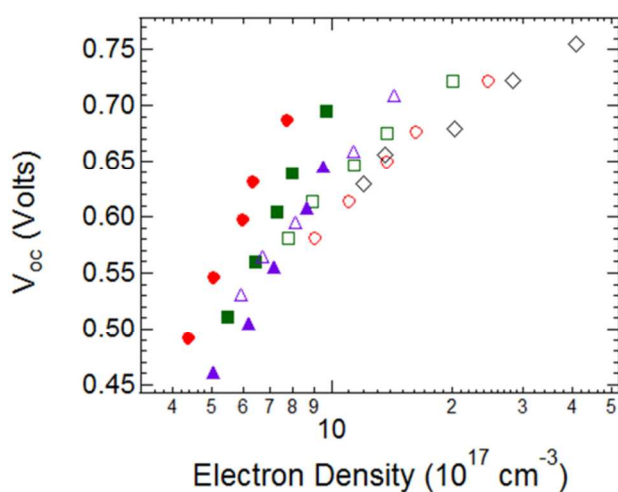
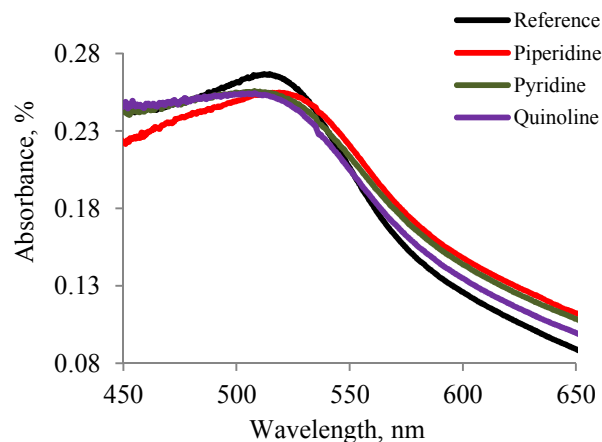


Fig. 9 Open-circuit voltage as a function of electron density in the TiO₂ film. Piperidine: ● - 150°C, ○ - 450°C; Pyridine: ■ - 150°C, □ - 450°C; Quinoline: ▲ - 150°C, △ - 450°C; and ◇ - Solaronix reference.

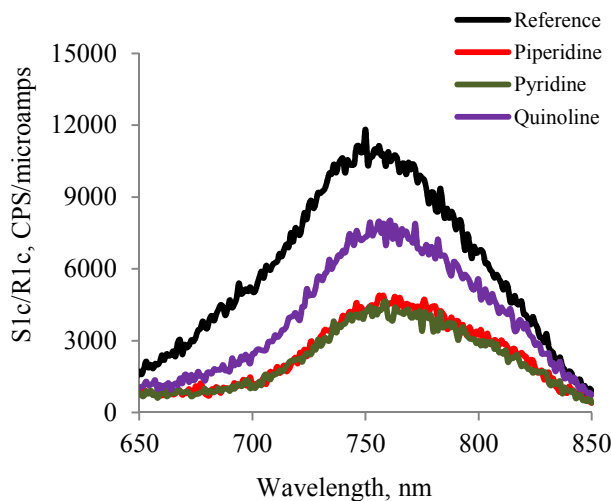
The absorbance and emission measurements of Al₂O₃ films prepared with the various heterocyclic bases and sensitized with N719 were measured (Figure 10) in order to investigate whether the traps caused by these bases also influence the device performance. The Al₂O₃ films were prepared using identical procedures to those for the TiO₂ films; however, the conduction band of Al₂O₃ is known to be too negative to allow electron injection from N719.⁵² Since electron injection cannot occur in these samples, they allow the dye excitation and relaxation process to be monitored directly.

Emission spectra from the films were obtained after excitation at 520 nm, with the absorbance spectra indicating identical absorption values at this wavelength. Since the number of absorbed photons is very similar and the dye is identical for all samples, the number of emitted photons would

be expected to be similar. However, the emission spectra indicate that luminescence from the films with bases were quenched compared to that without any nitrogen base. Further, the films prepared with pyridine and piperidine show a greater degree of quenching compared to those prepared with quinoline. This suggests that the excited state of the dye is deactivated in the presence of the bases, an effect which is more prominent for piperidine and pyridine than for quinoline. This trend is in agreement with the previous trends observed for the injection efficiency of devices, suggesting that in addition to conduction band shifts, the J_{sc} is influenced by deactivation of the dye excited state through interaction with the organic bases.



a)



b)

Fig. 10 a) Absorption of N719 and b) emission spectra of N719 excited at 520nm for Al₂O₃ films prepared with different binders.

The changes in the V_{oc} of the devices with various bases cannot be explained from the conduction band shifts observed in Figure 9, since these show the opposite trend to that expected. However, in addition to changes in the conduction band potential, the V_{oc} can also be influenced by changes in the electron density in the film due to injection or recombination.

To investigate the transport and recombination kinetics, the electron diffusion coefficient and lifetime were determined from photocurrent and photovoltage measurements, respectively (Figure 11). Little difference was observed in the diffusion coefficients as a function of J_{sc} between samples prepared with different bases, and the sintering temperature also did not show a large impact on the diffusion coefficients.

order quinoline > pyridine > piperidine. When the TiO_2 electrodes were sintered to $450^\circ C$, electron lifetime increases due to the reduction of TiO_2 bulk defects or the removal of organics which act as traps.

Finally, a comparison of the quantity effect of quinoline added either during the paste formulation or as a component in the electrolyte is under investigation

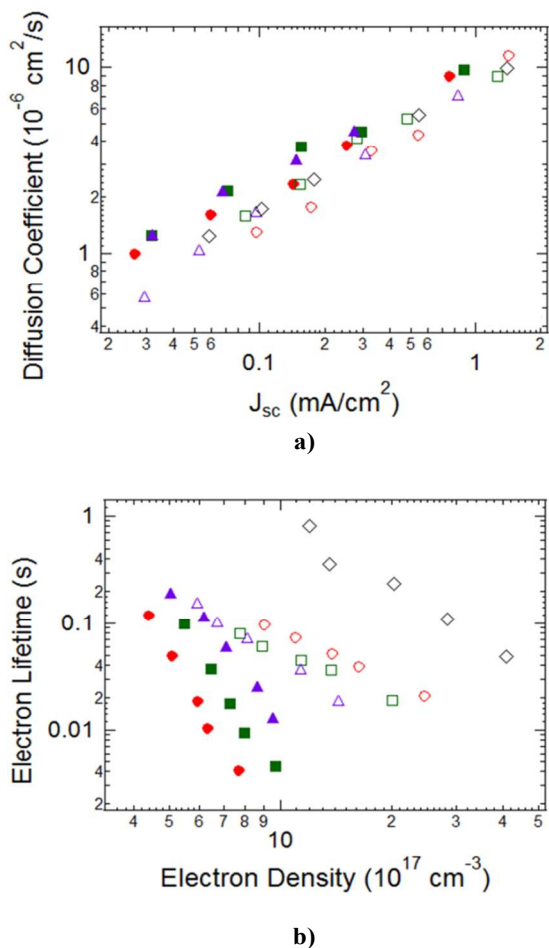


Fig. 11 a) Electron diffusion coefficient and b) electron lifetime of TiO_2 electrodes. Piperidine: ● - $150^\circ C$, ○ - $450^\circ C$; Pyridine: ■ - $150^\circ C$, □ - $450^\circ C$; Quinoline: ▲ - $150^\circ C$, △ - $450^\circ C$; and ◇ - Solaronix reference.

This indicates that the nature of the base within the electrode does not influence electron transport. However, electron lifetimes were observed to be different within the various electrodes. At low temperature, the electron lifetimes increase in the order piperidine < pyridine < quinoline when compared at the same electron density value. Since the density of traps is comparable between the various TiO_2 electrodes at $150^\circ C$ (the slopes of the V_{oc} vs ED plots are the same in Figure 9), these differences indicate less back electron transfer from TiO_2 to the electrolyte. The origin of this effect remains ambiguous, but could be caused either by steric hindrance of the surface with bulkier bases adsorbed or by a difference in the driving force for recombination (difference between TiO_2 conduction band and redox Fermi level) as the conduction band shifts between the bases. As a result of improved electron lifetime at low temperature, the device V_{oc} increases in the

Conclusions

In this study, we have demonstrated that low temperature TiO_2 colloidal pastes can be prepared with heterocyclic amines to produce robust 5 micron thick electrodes. Following a short thermal treatment of 15 minutes at $150^\circ C$, these single cast electrodes appear to have reasonable device efficiencies even though the elimination of organic species within TiO_2 electrodes is not complete. A simultaneous enhancement of J_{sc} and V_{oc} has been obtained by adding a more π -electron rich and bulkier heterocyclic base during paste formulation instead of introduction within electrolyte. The shift of the TiO_2 conduction band caused by varying basicity increased the electron injection efficiency and was predominantly responsible for the J_{sc} increase. However, the bases also deactivated the dye excited state, leading to small variations in the injection yield, and a significantly lower current than when the devices were heated to $450^\circ C$ to remove the bases. The more π -electron rich and bulkier heterocyclic bases also resulted in higher electron lifetimes induced by less electron recombination at the interface between TiO_2 /dye/electrolyte, resulting in small V_{oc} enhancements.

This methodology offers significant advantages in reducing costs by allowing TiO_2 colloidal pastes to become the material of choice when moving to roll-to-roll printing. Furthermore, since the pastes also show efficiencies over 6% after sintering at high temperatures, they offer a high degree of versatility and could be employed on either polymer, glass or metal foil substrates in DSSCs.

Acknowledgements

This research was carried out under funding provided by the Cooperative Research Centre for Polymers III. The authors wish to thank Dr Ian Dagley (CEO), and the participants of Project 3.1 and also acknowledge use of the facilities of Australian National Fabrication Facility (ANFF).

Notes and References

^a Institute of Materials Engineering, Australian Nuclear Science and Technology Organisation (ANSTO), Locked Bag 2001 Kirrawee DC NSW 2232, Australia. E-mail: gtx@ansto.gov.au; Tel: +61 2 97179070

^b ARC Centre of Excellence for Electromaterials Science and Intelligent Polymer Research Institute, AIIM Facility, University of Wollongong, Wollongong, NSW 2522, Australia

- 1 P. B. Weisz, *Phys. Today*, 2004, **57**, 47.
- 2 S. Chu and A. Majumdar, *Nature*, 2012, **488**, 294.
- 3 T. M. Razykov, C. S. Ferekides, D. Morel, E. Stefanakos, H. S. Ullal and H. M. Upadhyaya, *Sol. Energy*, 2011, **85**, 1580.
- 4 J. Kalowekamo and E. Baker, *Sol. Energy*, 2009, **83**, 1224.
- 5 J. B. Baxter, *J. Vac. Sci. Technol. A*, 2012, **30**, 020801.
- 6 S. Ito, T. N. Murakami, P. Comte, P. Liska, C. Gratzel, M. K. Nazeeruddin and M. Gratzel, *Thin Solid Films*, 2008, **516**, 4613.
- 7 R. Harikisun and H. Desilvestro, *Sol. Energy*, 2011, **85**, 1179.
- 8 G. E. Tulloch, *J. Photochem Photobiol. A*, 2004, **164**, 209.
- 9 B. O'Regan and M. Gratzel, *Nature*, 1991, **353**, 737.
- 10 L. M. Peter, *J. Phys. Chem. Lett.*, 2011, **2**, 1861.
- 11 J. Burschka, N. Pellet, S.-J. Moon R Humphry-Baker, P. Gao, M. K. Nazeeruddin and M. Gratzel, *Nature*, 2013, **499**, 316.
- 12 G. Hashmi, K. Miettunen, T. Peltola, J. Halme, I. Ashgar, K. Aitola, M. Toivola and P. Lund, *Renewable Sustainable Energy Rev.*, 2011, **15**, 3717.
- 13 T. Miyasaka, *J. Phys. Chem. Lett.*, 2011, **2**, 262.
- 14 S. Ito, P. Liska, P. Comte, R. Charvet, P. Pechy, U. Bach, L. Schmidt-Mende, S. M. Zakeeruddin, A. Kay, M. K. Nazeeruddin and M. Gratzel, *Chem. Commun.*, 2005, **34**, 4351.
- 15 T.N. Murakami, Y. Kijitori, N. Kawashima and T. Miyasaka, *J. Photochem. Photobiol. A*, 2004, **164**, 187.
- 16 D. Zhang, T. Yoshida, T. Oekermann, K. Furuta and H. Minoura, *Adv. Funct. Mater.*, 2006, **16**, 1228.
- 17 L.N. Lewis, J.L. Spivack, S. Gasaway, E.D. Williams, J. Y. Gui, V. Manivannan and O. P. Siclovan, *Sol. Energy Mater. Sol. Cells*, 2006, **90**, 1041.
- 18 J.A. Campbell, M. deBormiol, A. J. Mozer, P. J. Evans, R. P. Burford and G. Triani, *J. Vac. Sci. Technol. A*, 2012, **30**, 01A157-1.
- 19 H. C. Weerasinghe, P. M. Sirimanne, G. P. Simon and Y. B. Cheng, *Prog. Photovoltaics Res. Appl.*, 2012, **20**, 321.
- 20 T. Yamaguchi, N. Tobe, D. Matsumoto, T. Nagai and H. Arakawa, *Sol. Energy Mater. Sol. Cells*, 2010, **94**, 812.
- 21 M. Graetzel, R. A. J. Janssen, D. B. Mitzi and E. H. Sargent, *Nature*, 2012, **488**, 304.
- 22 N. G. Park, K. M. Kim, M. G. Kang, K. S. Ryu, S. H. Chang and Y. J. Shin, *Adv. Mater.*, 2005, **17**, 2349.
- 23 K. Kim, G. W. Lee, K. Yoo, D. Y. Kim, J. K. Kim and N. G. Park, *J. Photochem. Photobiol. A*, 2009, **204**, 144.
- 24 J. H. Yune, I. Karatchevseva, K. Wagner, D. Officer and G. Triani, *J. Mater. Res.*, 2013, **28**, 488.
- 25 S. Y. Huang, G. Schlichthorl, A. J. Nozik, M. Gratzel and A. J. Franck, *J. Phys. Chem. B*, 1997, **101**, 2576.
- 26 G. Boschloo, L. Häggman and A. Hagfeldt, *J. Phys. Chem. B*, 2006, **110**, 13144.
- 27 H. Kusama, M. Kurashige and H. Arakawa, *J. Photochem. Photobiol. A*, 2005, **169**, 169.
- 28 H. Kusama, Y. Konishi, H. Sugihara and H. Arakawa, *Sol. Energy Mater. Sol. Cells*, 2003, **80**, 167.
- 29 H. Kusama and H. Arakawa, *J. Photochem. Photobiol. A*, 2004, **165**, 15.
- 30 H. Kusama, H. Orita and H. Sugihara, *Sol. Energy Mater. Sol. Cells*, 2008, **92**, 84.
- 31 A.M. Asaduzzaman and G. Schreckenbach, *Phys. Chem. Chem. Phys.*, 2010, **12**, 14609.
- 32 I. Karatchevseva, D. J. Cassidy, Z. M. Zhang, G. Triani, K. S. Finnie, S. L. Cram and C. J. Barbe, *J. Am. Ceram. Soc.*, 2008, **91**, 2015.
- 33 T. X. Liu, F. B. Li and X. Z. Li, *J. Hazard. Mater.*, 2008, **155**, 90.
- 34 S. Winardi, R. R. Mukti, K. N. P. Kumar, J. Z. Wang, W. Wunderlich and T. Okubo, *Langmuir*, 2010, **26**, 4567.
- 35 N. W. Duffy, L. M. Peter, R. M. G. Rajapakse and K. G. U. Wijayantha, *Electrochem. Commun.*, 2000, **2**, 658.
- 36 S. Nakade, T. Kanzaki, Y. Wada and S. Yanagida, *Langmuir*, 2005, **21**, 10803.
- 37 H. Miyata, Y. Nakagawa, T. Ono and Y. Kubokawa, *J. Chem. Soc., Faraday Trans.*, 1983, **79**, 2343.
- 38 T. J. Dines, L. D. MacGregor and C. H. Rochester, *Langmuir*, 2002, **18**, 2300.
- 39 Socrates, G.; Infrared and Raman Characteristic Group Frequencies: Tables and Charts, John Wiley & Sons Hoboken, NY, 3rd edn, 2004.
- 40 M. Ni, M. K. H. Leung, D. Y. C. Leung and K. Sumathy, *Sol. Energy Mater. Sol. Cells*, 2006, **90**, 1331.
- 41 K. D. Benkstein, N. Kopidakis, J. van de Lagemaat and A. J. Frank, *J. Phys. Chem. B*, 2003, **107**, 7759.
- 42 A. B. F. Martinson, T. W. Hamann, M. J. Pellin and J. T. Hupp, *Chem. Eur. J.*, 2008, **14**, 4458.
- 43 S. K. Dhungel and J. G. Park, *Renewable Energy*, 2010, **35**, 2776.
- 44 S. Ahmed, A. Du Pasquier, T. Asefa and D. P. Birnie, *Adv. Energy Mater.*, 2011, **1**, 879.
- 45 K. S. W. Sing, D. H. Everett, R. A. W. Haul, L. Moscou, R. A. Pierotti, J. Rouquerol and T. Siemieniwska, *Pure Appl. Chem.*, 1985, **57**, 603.
- 46 T. Miyasaka and Y. Kijitori, *J. Electrochem. Soc.*, 2004, **151**, A1767.
- 47 D.R Lide, ed., CRC Handbook of Chemistry and Physics, Internet Version 2005, <<http://www.hbcpnetbase.com>>, CRC Press, Boca Raton, FL, 2005.
- 48 M. K. Brennaman, A. O. T. Patrocinio, W. Song, J. W. Jurss, J. J. Concepcion, P. G. Hoertz, M. C. Traub, N. Y. Murakami Iha and T. J. Meyer, *ChemSusChem.*, 2011, **4**, 216.
- 49 M. Grätzel, *Inorg. Chem.*, 2005, **44**, 6841.
- 50 R. Katoh, A. Huijser, K. Hara, T. J. Savenije and L. D. A. Siebbeles, *J. Phys. Chem. C*, 2007, **111**, 10741.
- 51 M. J. Griffith, A. J. Mozer, G. Tsekouras, Y. Dong, P. Wagner, K. Wagner, G. G. Wallace, S. Mori and D. L. Officer, *Appl. Phys. Lett.*, 2011, **98**, 163502.
- 52 S. E. Koops and J. R. Durrant, *Inorg. Chim. Acta*, 2008, **361**, 663.